Journal of Engineering Physics and Thermophysics, Vol. 72, No. 4, 1999

MODELING OF THE IMPACT DYNAMICS OF LARGE METEORIC BODIES ON THE SURFACE OF THE PLANET

F. N. Borovik, G. S. Romanov, and
A. S. Smetannikov

UDC 533.6.01

We present a procedure for numerical modeling and the results predicted for dynamics of crater formation in asteroid impact on the ground in the approximation of two-dimensional gas dynamics in an axisymmetric formulation. Gas-dynamic equations are solved using a fully conservative difference scheme in Eulerian variables. Predictions are performed with both an analytic representation of the equation of state (according to Tillotson) and wide-range semiempirical equations of state with a phase transition into vapor and a more exact specification of cold compression. Consideration is given to impact at a velocity of 50 km/sec with body dimensions of the order of 1 km.

Study of the dynamics of processes occurring in a high-velocity impact is of interest for many problems of astrophysics and space physics, namely, for creating systems of meteoritic defence of space vehicles and for studying meteoritic craters, the origin of planet atmospheres, possible consequences of the fall of large space objects onto the Earth, etc. Experimental data on high-velocity impact belong to the range of velocities no higher than 20 km/sec. The range of impact velocities of the order of 100 km/sec is practically inaccessible for experimental study (the only exception being the recent fall of the Shoemakers–Levy comet onto Jupiter at a velocity over 60 km/sec). As a consequence, theoretical study of impact dynamics (especially numerical modeling) gain particular importance for the range of higher impact velocities.

Gas-dynamic equations in $r-z$ coordinates under the condition of axial symmetry of the problem are of the following form:

$$\rho\left(\frac{\partial u}{\partial t}+v\frac{\partial u}{\partial r}+u\frac{\partial u}{\partial z}\right)=-\frac{\partial P}{\partial z},$$

$$\rho\left(\frac{\partial v}{\partial t}+v\frac{\partial v}{\partial r}+u\frac{\partial v}{\partial z}\right)=-\frac{\partial P}{\partial r},$$

$$\frac{1}{\rho}\frac{d\rho}{dt}=-\left[\frac{1}{r}\frac{\partial (rv)}{\partial r}+\frac{\partial u}{\partial z}\right], \tag{1}$$

$$\rho\frac{d\varepsilon}{dt}=-P\left[\frac{1}{r}\frac{\partial (rv)}{\partial r}+\frac{\partial u}{\partial z}\right].$$

The equation of state $P=P(\varepsilon, \rho)$ closes the system.

As previous investigations demonstrated, modeling of dynamics of asteroid penetration into the ground and of crater formation based on numerical schemes in Lagrangian coordinates causes certain difficulties because Lagrangian cells are strongly distorted in this problem. In numerical modeling of gas-dynamic problems in variables other than Lagrangian, terms that account for convective mass, momentum, and energy transfer appear in the equations. In this case, among the most important requirements specified for numerical algorithms is adherence to

Academic Scientific Complex "A. V. Luikov Heat and Mass Transfer Institute," National Academy of Sciences of Belarus, Minsk, Belarus. Translated from Inzhenerno-Fizicheskii Zhurnal, Vol. 72, No. 4, pp. 686-696, July-August, 1999. Original article submitted September 3, 1998.

 1062-0125/99/7204-0658$22.00

the conservation laws and balance relations involved in differential equations. Analyzing various difference schemes used in practice reveals that difference analogs of the convective terms therein do not satisfy the conservation conditions. These schemes have additional entropy sources and sinks resulting from uncoordination of the approximation of convective flows in the equations for mass, momentum, and energy variation. Fully conservative difference schemes (FCDS) in Lagrangian variables, developed previously [1], showed good quality of the solutions for a variety of entirely different problems. Their difference from conservative ones is that some additional relations are fulfilled (a balance among individual types of energy rather than only conservation of the total energy, etc.). Attempts to work out fully conservative difference schemes for the gas-dynamic equations in Eulerian variables for a long time failed. Study [2] ascertained that such schemes cannot be constructed using the quantities determined only on two temporal layers. Only afterward was the construction of FCDS in Eulerian coordinates (three-layer over time) a success. It was shown that convective flows of mass and internal energy should be matched [3]. Subsequently, multidimensional analogs of such schemes were also obtained [4].

We use a two-dimensional partially three-layer (with respect to velocity) FCDS in Eulerian cylindrical variables (r, z) based on these principles. In the scheme, i denotes the point number along the radius r, n is the point number along the axial coordinate z, and j is the index of the temporal layer. For simplifying the description we adopted the following designation [1]: $A = A^j$, $\hat{A} = A^{j+1}$, $\check{A} = A^{j-1}$, and $A^\alpha = \alpha\hat{A} + (1 - \alpha)A$. In the employed numerical scheme, magnitudes of the coordinates, velocities (r, z, v, u), and mass M relate to nodes of the net, and magnitudes of the density, energy, pressure, volume, and mass of the cell $(\rho, \varepsilon, P, V, m)$, to centers of the cells (these quantities are numbered by the left lower angle, i.e., $a_{i,n}$ corresponds to $a_{i+1/2,n+1/2}$). The volume, mass of the cell, and mass of the node are equal to

$$V_{i,n} = \frac{1}{2}(r_{i+1,n}^2 - r_{i,n}^2)(z_{i,n+1} - z_{i,n}); \quad m_{i,n} = (\rho V)_{i,n};$$

$$M_{i,n} = \frac{1}{4}(m_{i,n} + m_{i-1,n} + m_{i-1,n-1} + m_{i,n-1}).$$

The calculation of a temporal step is broken down into two stages, as is generally accepted for Eulerian procedure. At the first stage, we solved the equation for momentum components (the tilde indicates the value of a quantity obtained after the first calculation stage)

$$M_{i,n}\frac{[(\tilde{v} + v) - \check{(v + v)}_{i,n}]}{2\tau} = \frac{1}{2} r_{i,n}[(P_{i,n} - P_{i-1,n})(z_{i,n} - z_{i,n+1}) + (P_{i,n-1} - P_{i-1,n-1})(z_{i,n-1} - z_{i,n})], \tag{2}$$

$$M_{i,n}\frac{[(\tilde{u} + u) - \check{(u + u)}_{i,n}]}{2\tau} = -\frac{1}{4} r[(P_{i,n} - P_{i,n-1})(r_{i+1,n}^2 - r_{i,n}^2) + (P_{i-1,n} - P_{i-1,n-1})(r_{i,n}^2 - r_{i-1,n}^2)] \tag{3}$$

and the energy equation

$$m_{i,n}\frac{(\tilde{\varepsilon} - \varepsilon)_{i,n}}{\tau} = -\frac{1}{2} P_{i,n}\left\{[(rv^{0.5})_{i+1,n} - (rv^{0.5})_{i,n}](z_{i,n+1} - z_{i,n}) + (r_{i+1,n}^2 - r_{i,n}^2)(u_{i,n+1}^{0.5} - u_{i,n}^{0.5})\right\}, \tag{4}$$

in whose right-hand sides only the terms are left that relate to the pressure and, in fact, coincide with the equations of Lagrangian procedure. In these relations, $P = p^{\alpha} + q$, where p^{α} is the pressure "weighed" in time ($0 \le \alpha \le 1$), and q is the artificial viscosity, $v^{0.5} = (\tilde{v} + v)/2$, $u^{0.5} = (\tilde{u} + u)/2$.

The second stage takes into account the terms relating to convective transfer of a pertinent quantity in the equations of mass

$$\frac{(\hat{m} - m)_{i,n}}{\tau} = FX_{i,n+1/2} - FX_{i+1,n+1/2} + FY_{i+1/2,n} - FY_{i+1/2,n+1}, \tag{5}$$

energy

$$\frac{(\hat{m}\,\hat{\varepsilon} - m\,\tilde{\varepsilon})_{i,n}}{\tau} = \Psi X_{i,n+1/2} - \Psi X_{i+1,n+1/2} + \Psi Y_{i+1/2,n} - \Psi Y_{i+1/2,n+1}, \tag{6}$$

and momentum

$$\begin{aligned} \frac{[\hat{M}(\hat{v} + v) - M(\tilde{v} + v)]_{i,n}}{2\tau} &= \Phi X_{i-1/2,n} - \Phi X_{i+1/2,n} + \Phi Y_{i,n-1/2} - \Phi Y_{i,n+1/2}, \\ \frac{[\hat{M}(\hat{u} + u) - M(\tilde{u} + u)]_{i,n}}{2\tau} &= \overline{\Phi X}_{i-1/2,n} - \overline{\Phi X}_{i+1/2,n} + \overline{\Phi Y}_{i,n-1/2} - \overline{\Phi Y}_{i,n+1/2}. \end{aligned} \tag{7}$$

Here, the following expressions are used for relevant flows:

$$FX_{i,n+1/2} = \frac{1}{2}(r_{i,n+1} + r_{i,n})(\tilde{v}_{i,n+1} + \tilde{v}_{i,n})(z_{i,n+1} - z_{i,n})\rho_{i,n+1/2},$$

$$\rho_{i,n+1/2} = \begin{cases} \rho_{i-1,n}, & \tilde{v} \ge 0, \\ \rho_{i,n}, & \tilde{v} < 0; \end{cases}$$

$$FY_{i+1/2,n} = \frac{1}{4}(r_{i+1,n} + r_{i,n})(\tilde{u}_{i+1,n} + \tilde{u}_{i,n})(r_{i+1,n} - r_{i,n})\rho_{i+1/2,n},$$

$$\rho_{i+1/2,n} = \begin{cases} \rho_{i,n-1}, & \tilde{u} \ge 0, \\ \rho_{i,n}, & \tilde{u} < 0; \end{cases}$$

$$\Psi X_{i,n+1/2} = \frac{1}{4}(r_{i,n+1} + r_{i,n})(\tilde{v}_{i,n+1} + \tilde{v}_{i,n})(z_{i,n+1} - z_{i,n})(\rho\varepsilon)_{i,n+1/2},$$

$$(\rho\varepsilon)_{i,n+1/2} = \begin{cases} (\rho\varepsilon)_{i-1,n}, & \tilde{v} \ge 0, \\ (\rho\varepsilon)_{i,n}, & \tilde{v} < 0; \end{cases}$$

$$\Psi Y_{i+1/2,n} = \frac{1}{4}(r_{i+1,n} + r_{i,n})(u_{i+1,n} + u_{i,n})(r_{i+1,n} - r_{i,n})(\rho\varepsilon)_{i+1/2,n},$$

$$(\rho\varepsilon)_{i+1/2,n} = \begin{cases} (\rho\varepsilon)_{i,n-1}, & \tilde{u} \ge 0, \\ (\rho\varepsilon)_{i,n}, & \tilde{u} < 0; \end{cases}$$

$$\Phi X_{i+1/2,n} = \frac{1}{2}(\tilde{v}_{i,n} + \tilde{v}_{i+1,n})FX^{*}_{i+1/2,n}, \quad \overline{\Phi X}_{i+1/2,n} = \frac{1}{2}(\tilde{u}_{i,n} + \tilde{u}_{i+1,n})FX^{*}_{i+1/2,n},$$

$$\Phi Y_{i,n+1/2} = \frac{1}{2}(\tilde{v}_{i,n} + \tilde{v}_{i,n+1})FY^{*}_{i,n+1/2}, \quad \overline{\Phi Y}_{i,n+1/2} = \frac{1}{2}(\tilde{u}_{i,n} + \tilde{u}_{i,n+1})FY^{*}_{i,n+1/2},$$

$$FX^{*}_{i+1/2,n} = \frac{1}{4}(FX_{i,n-1/2} + FX_{i,n+1/2} + FX_{i+1,n-1/2} + FX_{i+1,n+1/2}),$$

$$FY^*_{i,n+1/2} = \frac{1}{4}\left(FY_{i-1/2,n} + FY_{i+1/2,n} + FY_{i-1/2,n+1} + FY_{i+1/2,n+1}\right),$$

At this stage, a definitive transition from parameters on the given and former temporal layers to parameters on the new temporal layer is accomplished. Introducing the quantities FX^* and FY^* and representing them in terms of the flows ΦX, ΦY, $\overline{\Phi X}$, and $\overline{\Phi Y}$ (matching of the flows) allows satisfaction of the principle of conservation [3]. It should be noted that a somewhat different definition of the quantities $(\rho\varepsilon)$ that is compatible with the principles of full conservation is possible.

For closing the system of gasdynamic equations it is necessary to assign the equation of state of media, i.e., to define the pressure and temperature as functions of the energy and density. In calculations we used the Mie–Grüneisen equation of state in the form proposed by Tillotson [5]. For material density larger than the normal density of a solid body $\rho \geq \rho_0$ we assumed the relation

$$p = \left[a + \frac{b}{1 + \varepsilon/(\varepsilon_0\delta^2)}\right]\rho\varepsilon + A\mu + B\mu^2.$$

With density smaller than that of a solid body $\rho \leq \rho_0$ we used the equation

$$p = a\rho\varepsilon + \left[\frac{b\rho\varepsilon}{1 + \varepsilon/(\varepsilon_0\delta^2)} + A\mu\exp\left[-\beta\left(\frac{1}{\delta} - 1\right)\right]\right]\exp\left[-\alpha\left(\frac{1}{\delta} - 1\right)^2\right].$$

In these expressions, $\delta = \rho/\rho_0$ and $\mu = \delta - 1$. In calculations with the Tillotson equation of state, gabbroid anartosite was taken to be the meteorite and ground material, to which the following parameters correspond: $a = 0.5$, $b = 0.11$, $\varepsilon_0 = 9.1$ MJ/kg, $A = 70.5$ GPa, $B = 135$ GPa, $\rho_0 = 2.94$ kg/dm^3, $\alpha = 5$, and $\beta = 10$. Besides, wide-range semiempirical equations of state for SiO_2 are used for describing granite (the meteriote and ground) [6, 7]. Thermodynamic parameters are calculated on the basis of resolving the pressure and energy into cold and thermal (nuclear and electronic) components [8]. Thermal electronic components of the energy and pressure were calculated on the basis of the Thomas–Fermi model for the average charge $Z = 10$ [8]. The pressure on a cold isotherm for $\rho < \rho_{0k}$ ($\rho_{0k} = 2.59$ kg/dm^3) was specified in the form $P_c = A(\delta^\sigma - \delta^\nu)$, $\delta = \rho/\rho_{0k}$. For ν we assumed a value of 5/3. Magnitudes of A and σ were determined from the known sound speed and sublimation energy: $\sigma = 3.115$ and $A = 24.8$ GPa. For compressions from 1 to 3 we used a cold isotherm [6] that takes into account experimental data. For greater compressions it was joined with a cold isotherm of the Thomas–Fermi model with correlations calculated for the average charge $Z = 10$. The thermal free energy of a nuclear component of the material consists of three terms describing the condensed state (within the framework of the Einstein model), evaporation, and dissociation. The following expressions were obtained from it for the pressure and energy:

$$P = \left[9\gamma - (9\gamma - 1)\frac{z_1^{n_1}}{1 + z_1^{n_1}} + \frac{2z_2^{n_2}}{1 + z_2^{n_2}}\right]\frac{\rho RT}{M}, \quad E = E_* - 6.5\,\frac{RT}{M}\frac{z_1^{n_1}}{1 + z_1^{n_1}} - \left(\frac{2RT}{M} - Q\right)\frac{z_2^{n_2}}{1 + z_2^{n_2}},$$

where $Q = 21.1$ MJ/kg is the dissociation of a SiO_2 molecule. Here,

$$E_* = a_1 + a_2T + a_3T^2, \text{ if } T < T_*, \quad E_* = b_1 + b_2T, \text{ if } T > T_*,$$

$$z_1 = \frac{0.0266}{\theta_0\rho^{9\gamma-1}}\theta_1\theta_2^2\theta_3T^{5/2}\rho_0^{9\gamma}, \quad z_2 = \theta_1\theta_2^2\theta_3\frac{13.36}{T^2\rho^2}\exp\left(-\frac{QM}{RT}\right),$$

where $T_* = 680$ K, $a_1 = -8.31\cdot10^3$ J/kg, $a_2 = 66.9$ J/(kg·K), $a_3 = 1.185$ J/(kg·K^2), $b_1 = -55.7$ J/kg, $b_2 = 1.67\cdot10^3$ J/(kg·K), $\theta_1 = 1351$ K, $\theta_2 = 603$ K, $\theta_3 = 1780$ K, $\gamma = 2/3$, $\theta_0 = 600$ K, $\rho_0 = 2.57$ kg/dm^3, $n_1 = 0.25$, and $n_2 = 0.2$ [6, 7]. Calculations based on the above-stated model yielded the following parameters of the critical point: $T =$

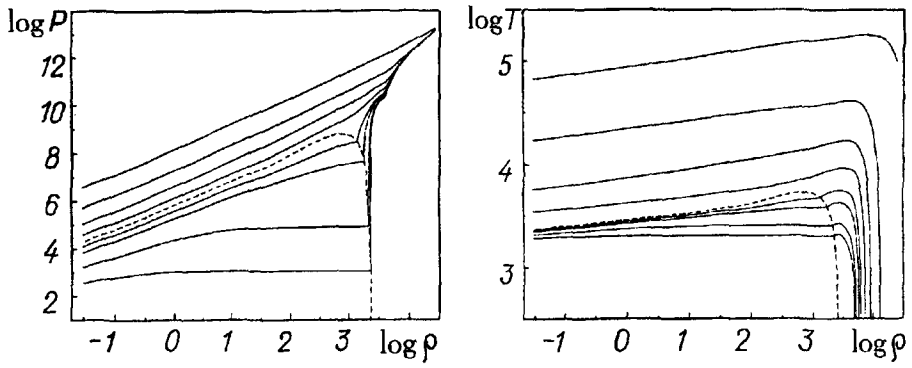

Fig. 1. Pressure and temperature vs. density for the set of energies (3, 4, 7, 10, 20, 40, 100, 600 MJ/kg, upward) by semiempirical equations of state. P, Pa, ρ, kg/m^3; T, K.

5386 K, $\rho = 0.75$ kg/dm^3, and $P = 0.51$ GPa. The equations of state, derived from these expressions, are shown in Fig. 1, which plots isoenergy curves and a binodal calculated on the basis of the Maxwell rule (a dashed line).

We performed test calculations of the dynamics of high-velocity impact for a wide range of impact velocities and dimensions of the striker using the equations of state both for ideal gas and in Tillotson's form. Comparing the results of our calculations of the impact of an aluminum striker on an aluminum target showed quite satisfactory agreement with previous calculated results and experimental data [9]. For fairly long times, the numerical solution approaches self-similar relations (by the profiles of quantities, by the time variation of axial and radial components of the momentum, etc.).

We next proceed to calculations of the meteorite impact on the ground. The meteorite (the striker) was modeled by a cylinder of diameter D and height H that collides with the ground with velocity u_0 normal to the surface. We specifically consider the following calculation versions:

1) $D = H = 1$ km, the initial velocity is $u_0 = -50$ km/sec, densities of the meteorite and ground are equal to 2.94 kg/dm^3, and the equation of state is taken in Tillotson's form;

2) similar to version 1 but the striker dimensions are twice as large $D = H = 2$ km;

3) similar to version 1 but wide-range semiempirical relations are used as the equations of state; densities of the meteorite and ground are equal to 2.57 kg/dm^3.

The pressure at the initial instant of time is 1 atm (ground, striker, and gas). The gas–ground contact boundary lies at $z = 0$, positive z correspond to the gas, and negative to the ground. At the initial instant of time the meteorite comes in contact with the ground. It should be noted that in the relief region (at densities somewhat smaller than the density of a solid body ρ_0) the Tillotson equations of state gives very large negative pressures (at low energies). In fact, when the negative pressure exceeds a magnitude of the order of 0.1 GPa there occurs a splitting off (a breaking), and the pressure goes to zero. In this connection, when it turned out that the pressure was lower than -0.1 GPa we assumed that $p = 0$. A similar procedure in this parametric region was employed in [9].

The difference net is constructed such that there is a satisfactory spatial resolution near the region of the initial position of the striker (where actually a crater is formed) and at the same time the flow can be traced at fairly large distances from the place of impact. For this end, in the striker region the net is constructed with a constant step along radial and axial coordinates, and in the remaining region the cell size increases in geometric proportion with a coefficient of 1.05–1.1 with respect to the distance from the initial position of the striker. For evaluation of the melted and evaporated mass upon impact we adopted the density of internal energy corresponding to melting $\varepsilon_m = 1.5$ MJ/kg and to evaporation $\varepsilon_e = 11.7$ MJ/kg. For the striker mass M_0 and velocity u_0 the maximal possible melted mass (in masses of the striker) is $M_m'/M_0 = u_0^2/(2\varepsilon_m)$. For the assigned values $u_0 = 50$ km/sec and $\varepsilon_m = 1.5$ MJ/kg we obtain a melted mass of $M_m'/M = 833$. An analogous evaluation for a maximal evaporated mass yields $M_e'/M_0 = u_0^2/(2\varepsilon_e) = 107$. These estimates are obtained proceeding from the condition that the entire kinetic energy is spent on melting (or evaporation). In the calculation, at each given instant of time we will determine the

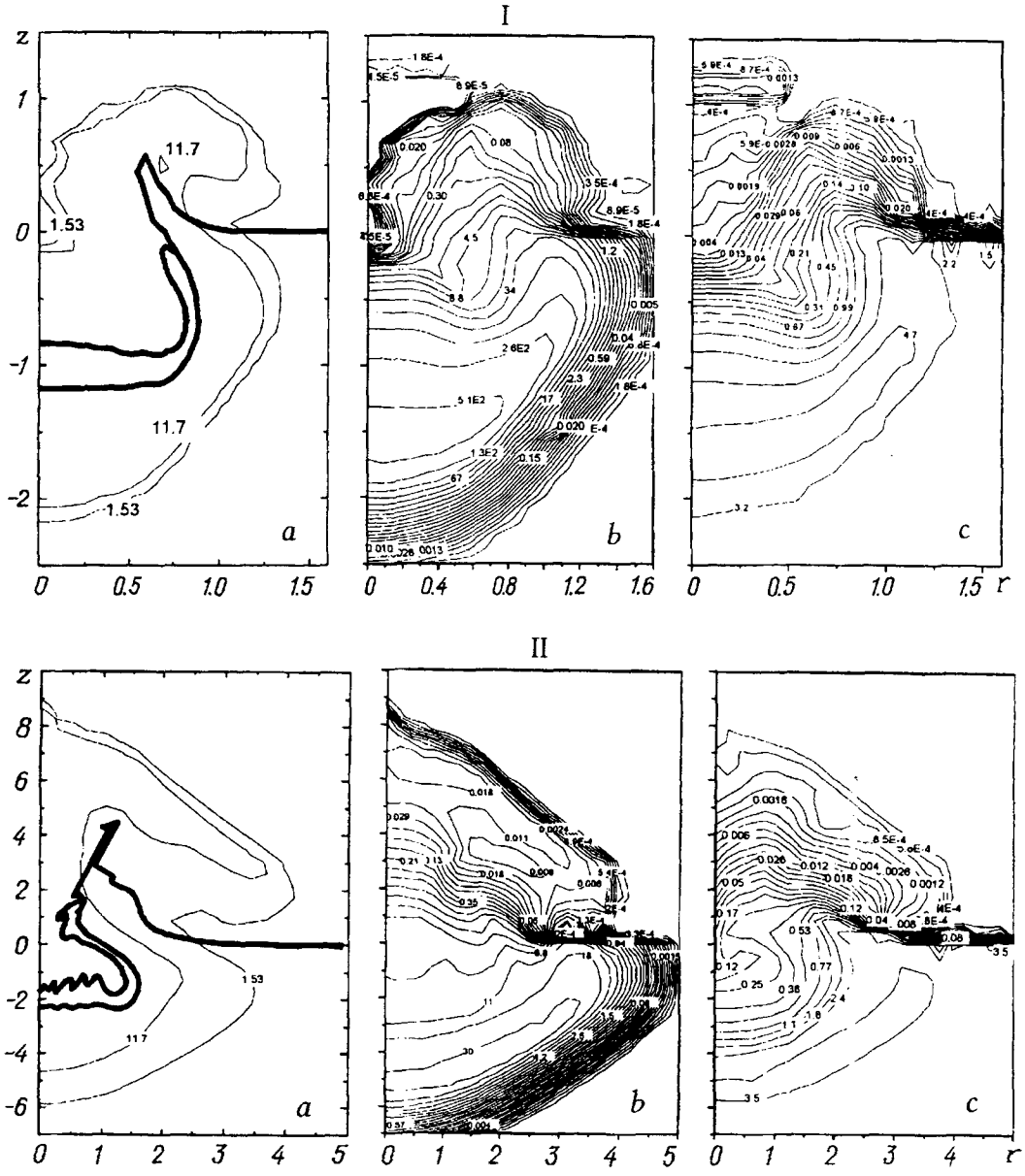

Fig. 2. Flow parameters for $t = 0.05$ sec (I) and $t = 0.3$ sec (II) (1st version): position of the contact boundaries (heavy lines) and isolines conforming to the melting and evaporation energy, MJ/kg (a); pressure field, GPa (b); and density field, kg/dm^3 (c). z, r, km.

cell mass M_e, where the specific energy is higher than the evaporation energy, and the cell mass M_m, where the specific energy is higher than the melting energy.

We next discuss the results calculated by the first version. At the place of impact the pressure increases rapidly and is 1950 GPa (0.023 sec) at a maximum. Two shock waves arise on the axis of symmetry; one goes deep into the ground and the other propagates over the striker body in the direction toward its motion. In an instant of 0.05 sec, the maximal pressure decreases to 623 GPa, the internal energy has a maximal value of 220 MJ/kg, and the maximal density is 5.95 kg/dm^3. The shock wave going over the striker body rapidly increases the specific energy of the material and evaporates it. The shock wave moving into the ground has a velocity of about -20 km/sec and is situated at $z = -1.6$ km. Here, on the axis of symmetry the striker–ground contact boundary reached $z = -11.15$ km, the striker–gas contact boundary attained $z = -0.84$ km (on the z axis), and the radial dimension of the crater increased to 1 km. By this instant of time the meteorite body is turned inside out, i.e., the outer surface of the striker (making contact with the gas at the initial instant of time) becomes inner, and the inner surface

(making contact with the ground at the initial instant of time) becomes outer. An upward jet generates over the edge of the formed crater. Here also emerge "tendrils" of the ground material thrown into the gas. Figure 2, I presents the position of contact boundaries (a) and pressure (b) and density (c) isolines at the instant of 0.05 sec. An intricate flow pattern is formed. The striker body and the inflowing gas move into the ground, and in the ground lying below the striker this flow begins to diverge along the radius. Over the edge of the formed crater, an upward jet arises that spreads out radially at a height of about 1 km. A part of the material in the jet acquires significant velocity components directed toward the axis of symmetry in the rarefied region formed after the striker. Subsequently, the flow cumulates on the axis of symmetry, and as a result, the density of internal energy (and temperature) in this region rises significantly, up to 420 MJ/kg (0.1 sec). A hot jet of the gas ascends a height of about 2 km by the instant of 0.1 sec. At the same time, a pressure and density maximum remains in the shock wave propagating in the ground; it amounts to 224 GPa and 5.15 kg/dm^3 and is located at a certain distance from the axis of symmetry. The velocity of the shock wave on the axis of symmetry is 9 km/sec. The depth of the crater increases by this instant of time up to 1.8 km, and the radial dimension up to 1.3 km. Further on, the flow keeps developing and the crater enlarges. By the instant of 0.3 sec, the striker–ground contact boundary reaches a maximal depth of 2.2 km. The evaporated meteorite material in the lower part of the crater starts moving toward the gas. Here Rayleigh–Taylor instability is likely to develop, since a more dense material accelerates toward a less dense. A detailed study of this process probably requires a better net resolution, which we did not achieve. The crater dimensions by this instant of time are as follows: the depth is 3 km and the radius is 2 km. Figure 2, II presents the fields of various quantities at a time of 0.3 sec. The hot region in the gas ascends a height of about 7 km, and the maximum of the specifc energy is 230 MJ/kg. The maximal pressure in the shock wave propagating over the ground is 48 GPa. Subsequent development leads to enlargement of the region covered by the flow and to gradual decrease of the maximal parameters. At $t = 2$ sec, the pressure maximum in the shock wave is 3.53 GPa, the hot region in the gas has risen to a height of about 40 km, and the maximum of the specific energy therein is 48.6 MJ/kg. By this instant of time the crater depth is 6 km and the radius is 5 km.

The time variation of various integral characteristics is presented in Fig. 3, the 1st version. The following quantities are shown: internal (in) and kinetic (k) energies (a); evaporated mass (e) and melted mass (m), all in masses of the meteorite (b); axial (I_z) and radial (I_r) components of the momentum (c); and total energy of the cells with the specific energy larger than the evaporation energy (e) and the melting energy (m) (d). All quantities are related to the initial energy of the striker $E_0 = M_0 u_0^2/2$. While penetrating into the ground, the striker decelerates and the kinetic energy converts rapidly to internal. By the instant of 0.16 sec the internal energy is at a maximum and makes up 70% of the initial energy of the striker. Subsequently, it falls slowly and the kinetic energy rises. At $t = 1.7$ sec they become equal. The evaporated mass attains a maximum at $t = 0.13$ sec and comprises 24.9 masses of the meteorite. A maximum of the melted mass (131.5 M_0) is formed noticeably later, at 0.3 sec. The magnitude of the melted mass remains nearly constant up to 1.3 sec and is larger than 100 M_0. The time dependence of axial and radial components of the momentum gradually becomes a self-similar law with an index of 0.59. Already for a time larger than 0.3 sec this relation is practically fulfilled. The portion of the internal energy contained in the evaporated material increases rapidly, becomes maximal at 0.087 sec (0.645), and then falls to a magnitude smaller than 0.1 for a time longer than 0.6 sec. The similar value for cells with energy higher than the melting energy attains a maximum somewhat later, at 0.166 sec, and is equal to 0.696. This value is practically the same as the maximum of the internal energy, making up 0.7 of the total energy. Thereafter the energy portion in the melt decreases to a value below 0.5 for a time longer than 0.42 sec. The portion of the internal energy at this instant of time is higher and equal to 0.66. Further on, this discrepancy becomes greater, since the energy contained in the melt rapidly decreases in time, and the internal energy falls very slowly. It should be remarked that the energy portion in the material raised above $z = 0$ is smaller than 0.1.

Because the flow pattern in the second calculation version is qualitatively similar to the foregoing version, we will not describe it in detail. It should only be noted that the initial kinetic energy of the striker E_0 is increased by 8 times (owing to dimensions) in comparison with the first version. Figure 3 (the 2nd version) plots the time variation of integral characteristics of the flow. The maximal internal energy is $0.7E_0$ and is attained at $t = 0.4$ sec. The time variation of the evaporated and melted masses is qualitatively similar to the first version, and here the

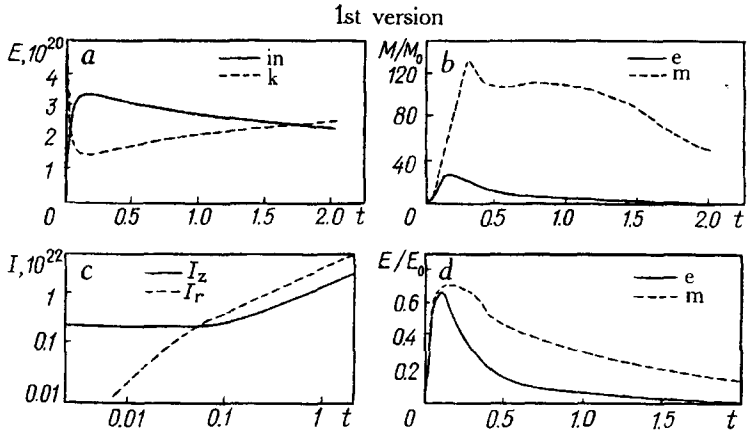

evaporated mass attains a maximum of about 0.2 of M_e', and the melted mass about 0.16 of M_m'. It should also be

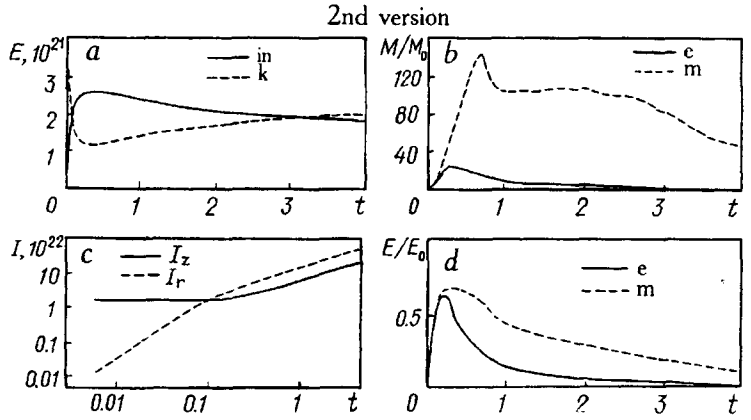

Fig. 3. Temporal behavior of integral characteristics for the 1st and 2nd calculation versions: internal and kinetic energies (a), evaporated and melted masses (b), radial and axial momenta (c), and energy portion in the melted and evaporated materials (d). E, J; I, g·cm/sec; t, sec.

noted that an increase in the striker energy leads to a later attainment of the maximum of the evaporated and melted masses. Figure 3d (the 2nd version) illustrates the time variation of the energy contained in the evaporated and melted materials (relative to the initial energy of the striker E_0). An energy increase owing to the striker dimensions (versions 1 and 2) indicates a similar temporal behavior of the relative energy in the evaporated and melted materials; only the characteristic time increases by twofold in proportion to $E_0^{1/3}$. The crater dimensions in the 2nd calculation version (a radius of 10 km and a depth of 11 km for $t = 4$ sec) doubled in comparison with the first version, i.e., the dimensions were retained in reduced coordinates $r' = r/E_0^{1/3}$ for the same reduced instant of time $t' = t/E_0^{1/3}$.

We now consider results of the third calculation version, which uses wide-range semiempirical equations of state. The flow develops like in the first calculation version. Figure 4, I presents pressure, density, and temperature fields for an instant of time of 0.05 sec. The spatial distribution of these quantities is close to that obtained in the first calculation version. The maximal temperature at $t = 0.05$ sec is above 6 eV, and the region with a temperature above 6.1 eV lies near the axis of symmetry at a depth ranging from -1 to -1.5 km and stretches radially for up to 0.6 km. The maximal pressure in the shock wave propagating over the ground is 510 GPa. The flow development leads to a gradual decrease in the parameters. By the instant of time of 0.3 sec the maximal pressure falls to 25 GPa, and the maximal temperature to 3.7 eV. The pressure, density, and energy distributions for this instant of time (Fig. 4, II) are similar to those obtained in the first version and the maximal values practically coincide. At the same time, the flow develops more slowly than in the calculation with the Tillotson equation of state, and the region involved in the motion appears to be somewhat smaller. Figure 5 shows the

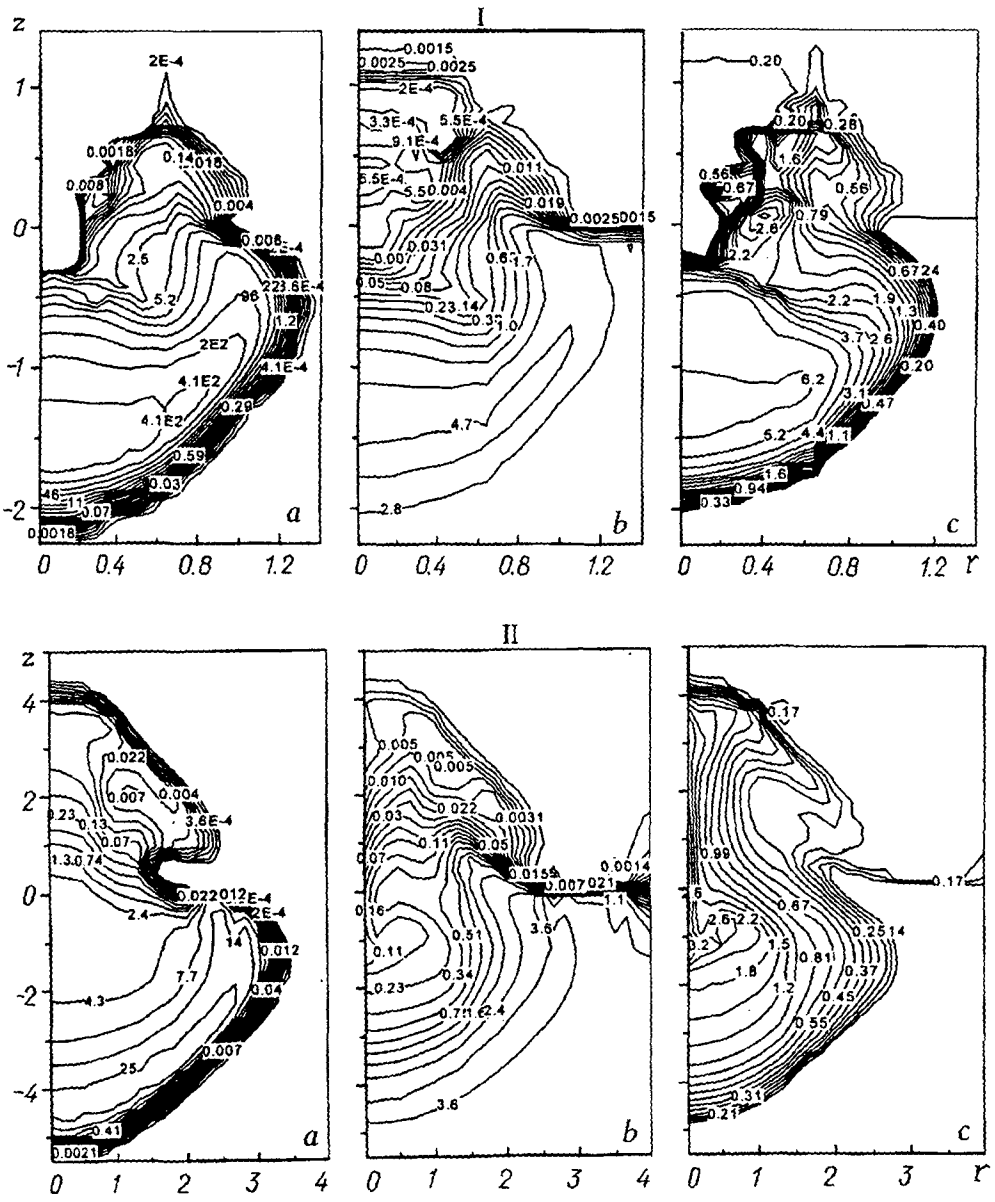

Fig. 4. Flow parameters for $t = 0.05$ sec (I) and $t = 0.3$ sec (II) (3rd version): a) pressure, b) density, and c) temperature fields.

temporal behavior of integral characteristics of the flow for this calculation version (values of the presented quantities are the same as in Fig. 3). While penetrating into the ground, the striker slows down and by $t = 0.25$ sec over 2/3 of the initial kinetic energy transforms into internal. The mass of evaporated material attains a maximum of 26 M_0 (0.2 sec) and thereafter falls. The mass of the melted material increases up to a maximum of 204 M_0 (0.5 sec), decreases to 150 M_0 (0.8 sec), and afterward slowly increases again. The temporal behavior of radial and axial momenta is similar to the first version. The energy contained in the evaporated material attains a maximum of 0.67 E_0 (0.12 sec) and then falls. The energy contained in the melted material increases to 0.8 E_0 (t = 0.5 sec), thereafter decreases, and up to 2 sec remains practically unchanged, amounting to about 0.7 E_0. Comparing with the first calculation version we should note the main difference, namely, while in the first version the internal energy attains a maximum and thereafter falls, becoming equal to kinetic at 1.7 sec, in the third version the internal and kinetic energies remain practically constant starting from 0.25 up to 2 sec. The difference in the temporal behavior of the melt mass and energy is also linked with this factor.

The following should be noted in conclusion. We worked out a computational program for two-dimensional gasdynamic problems based on fully conservative difference schemes in Eulerian coordinates with a matched approximation of the flows. The calculations of various test problems indicated a satisfactory quality of the solutions

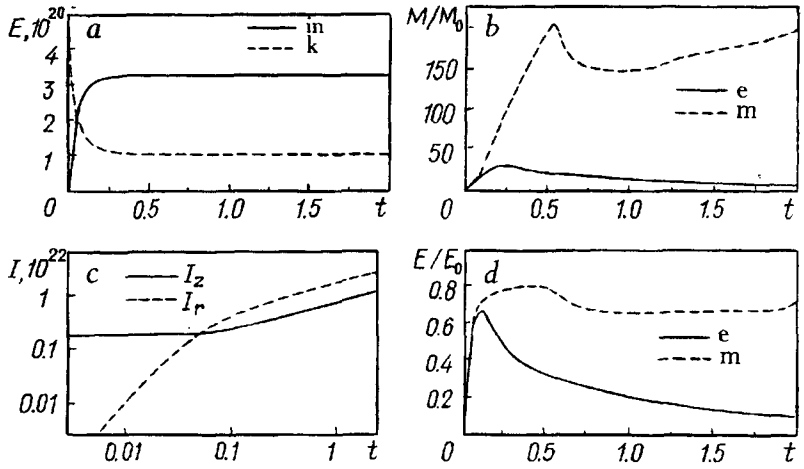

Fig. 5. Temporal behavior of integral characteristics for the 3rd calculation version.

obtained using this procedure. We performed numerical modeling of the dynamics of crater formation as a result of meteorite impact on the ground. The calculated results allowed detailed consideration of the deformation of the meteorite body and the dynamics of crater formation and flow in the surrounding medium. The calculations reveal that an increase in radial dimensions of the crater lasts noticeably longer than does attainment of a maximal depth of penetration by the striker. For a striker 1 km in diameter, 1 km long, and with a velocity of 50 km/sec, the maximal depth of penetration into the ground (2.2 km) is reached at 0.18 sec, and for a time of 2 sec the radial expansion still persists. Comparing the results calculated for an impact with the same velocity but with different dimensions of the striker attests to a similarity in the flow characteristics. Here, the characteristic time and distance vary in proportion to the energy to a power of 1/3, and the relative masses M/M_0 and energies E/E_0 prove to be the same at equal reduced instants of time $t' = t/E_0^{1/3}$. Comparing the calculations with different equations of state (those of Tillotson and semiempirical ones with allowance for evaporation) manifests that while in the initial phase (the striker penetration into the ground and deceleration) the results turn out to be close, subsequent development of the flow differs markedly.

The work was carried out with financial support from the International Scientific Technical Center (project V-23-96).

NOTATION

r, z, coordinates; t, time; v, u, radial and axial velocity components; ρ, density; P, pressure; ε, energy of unit mass; T, temperature; R, gas constant; M, molecular weight; Q, dissociation energy; ρ_{0k}, normal density at $T = 0$ K; ρ_0, normal density; γ, Grüneisen coefficient; θ_0, Debye temperature at normal density; σ and ν, exponents in the pressure–compression relation on the zeroth isotherm. Subscripts: m, melted material; e, evaporated material; c, cold components of the equation of state; i, number of the point along the radius; n, number of the point along the axis; j, number of the temporal layer.

REFERENCES

1. A. A. Samarskii and Yu. P. Popov, *Difference Methods of Solution of Gas-Dynamic Problems* [in Russian], Moscow (1980).
2. A. V. Kuz'min, V. L. Makarov, and G. V. Meladze, *Zh. Vych. Mat. Mat. Fiz.*, **20**, No. 1, 171-181 (1980).
3. V. M. Goloviznin, M. A. Ryazanov, A. A. Samarskii, and O. S. Sorokovnikova, *Dokl. Akad. Nauk SSSR*, **274**, No. 3, 524-528 (1984).
4. V. M. Goloviznin, M. A. Ryazanov, A. A. Samarskii, et al., *Computational Methods in Mathematical Physics* [in Russian], Moscow (1986), pp. 5-41.

5. J. D. O'Keefe and T. J. Ahrens, *Proc. Lunar Sci. Conf.*, 6th (1975), pp. 2831-2844.
6. S. V. Bobrovskii, V. M. Gogolev, B. V. Zamyshlyaev, et al., *Fiz.-Tekh. Probl. Razrab. Polezn. Iskop.*, No. 2, 58-61 (1976).
7. S. V. Bobrovskii, V. M. Gogolev, B. V. Zamyshlyaev, et al., *Fiz.-Tekh. Probl. Razrab. Polezn. Iskop.*, No. 3, 49-57 (1976).
8. N. N. Kalitkin and L. V. Kuz'mina, Tables of Thermodynamic Functions of Material at High Energy Concentration [in Russian], *Preprint No. 35*, Institute of Applied Mathematics of the USSR, Academy of Sciences, Moscow (1975).
9. J. K. Dienes and J. M. Walsh, *High-Velocity Impact Phenomena*, New York (1970).